Lab on a Chip

PAPER

A high throughput molecular force assay for protein–DNA interactions†

Philip M. D. Severin, Dominik Ho and Hermann E. Gaub*

An accurate and genome-wide characterization of protein–DNA interactions such as transcription factor binding is of utmost importance for modern biology. Powerful screening methods emerged. But the vast majority of these techniques depend on special labels or markers against the ligand of interest and moreover most of them are not suitable for detecting low-affinity binders. In this article a molecular force assay is described based on measuring comparative unbinding forces of biomolecules for the detection of protein–DNA interactions. The measurement of binding or unbinding forces has several unique advantages in biological applications since the interaction between certain molecules and not the mere presence of one of them is detected. No label or marker against the protein is needed and only specifically bound ligands are detected. In addition the force-based assay permits the detection of ligands over a broad range of affinities in a crowded and opaque ambient environment. We demonstrate that the molecular force assay allows highly sensitive and fast detection of protein–DNA interactions. As a proof of principle, binding of the protein EcoRI to its DNA recognition sequence is measured and the corresponding dissociation constant in the sub-nanomolar range is determined. Furthermore, we introduce a new, simplified setup employing FRET pairs on the molecular level and standard epi-fluorescence for readout. Due to these advancements we can now demonstrate that a feature size of a few microns is sufficient for the measurement process. This will open a new paradigm in high-throughput screening with all the advantages of force-based ligand detection.

Introduction

DNA-binding proteins coordinate a variety of fundamental functions in cells such as transcriptional regulation, replication and DNA repair. For instance the interactions between transcription factors and their DNA binding sites are an essential part of the gene regulatory networks that control development, core cellular processes and responses to environmental perturbations. These networks and systems may exhibit interactions between as many as thousands of unique elements. A profound understanding of protein–DNA interactions as well as their quantitative evaluation is therefore of utmost importance for modern molecular and systems biology. As a consequence, many different high-throughput methods for the characterization of protein–DNA interactions emerged over the last decade. The most prominent representatives are chromatin immunoprecipitation on a DNA-chip (ChIP-chip)[1–3] and protein binding microarrays (PBMs).[4,5] Both techniques are well established and thanks to microarray technology capable of high-throughput. But despite of all advantages to identify *in vivo* locations, ChIP-chip has some inherent challenges that can make the

identification of DNA-binding sites delicate.[6,7] Especially, both condition-specific binding and antibody limitations may prevent sufficient enrichment of bound fragments in the immunoprecipitated sample.[7,8] PBMs in turn are limited by their stringent washing requirements, which may cause loss of weakly bound proteins. This impairs the determination of transient and low-affinity binding sites. But for instance during fly embryonic development these very sites are suggested to contribute as much as high-affinity sites.[9] To solve this issue the Quake group introduced an *in vitro* assay that mechanically trapped the interacting molecules (MITOMI).[10]

What ChIP-chip, PBMs and MITOMI have in common, is the need of an antibody against the DNA binding protein of choice or against an epitope-tag of this protein. Either the protein is fished out like in ChIP-chip or MITOMI, or it is marked with a fluorescent antibody for detection like in PBMs. So in addition to the binding DNA sequence these established methods rely on a second binding partner specific against the DNA-binding protein. Hence it follows: first, the success and vulnerability of these assays depend on the affinity and specificity of the antibodies. Second, the DNA-binding protein must have a common tag, or, if not, an antibody with high specificity against the protein must be available.

A different approach for the detection of protein–DNA interactions evolved in recent years with the advancement of single molecule force spectroscopy.[11–14] In single molecule force

Lehrstuhl für Angewandte Physik and Center for Nanoscience (CeNS), Ludwig-Maximilians-Universität, Amalienstrasse 54, 80799 Munich, Germany. E-mail: gaub@physik.uni-muenchen.de; Fax: +49 89-2180-2050
† Electronic supplementary information (ESI) available: Preparation of DNA-chip and PDMS-stamp. See DOI: 10.1039/c0lc00302f

spectroscopy a variety of experimental tools based on measuring and applying forces between molecules in the piconewton regime have been developed and have contributed to a better understanding of the mechanics of biomolecules and molecular bonds.[15–18] However, there are two major bottlenecks, which have hindered the widespread use of single-molecule mechanics: sizable instrumental effort and limited force resolution. To solve these issues a new technique, the molecular force assay (MFA), has been introduced by our group.[19,20] The MFA measures unbinding forces with a high sensitivity like single mismatches in DNA[21] and with low-budget and simple instrumentation compared to AFM, optical or magnetic tweezers. Since with the state-of-the-art instrumentation the force resolution is limited only by thermal fluctuations of the force sensor, shrinking the sensor size improves the signal-to-noise ratio.[22,23] Instead of a trapped bead or a microscopic cantilever, MFA employs a precisely defined bond like a DNA duplex as force sensor. To increase the precision even further, the assay is built in a comparative measurement format, where rupture forces of two molecular complexes are directly compared with each other. The difference in stability of the two bonds is then translated into a fluorescent signal. In contrast to other single molecule force techniques, the MFA has a high degree of parallelization of force sensors built up in a chip-like format, which allows to test in the order of 10^4 per µm^2 molecular force probes (MFPs).[24] But although a large number of molecules are probed simultaneously, the actual force measurement is still performed at the single molecule level, because each sample bond is probed individually by a single reference bond.[19]

In our previous work we could demonstrate the advantages of the MFA for label-free ligand detection of small binding molecules like hairpin polyamides[24,25] or adenosine *via* an aptamer-based sensor[26] in a molecular crowded environment with dissociation constants reaching from pM to mM concentrations. The assays permitted up to 16 distinct force sensors to be placed in 16 different spots (diameter 1–2 mm) per experiment on a DNA-chip. After several washing and incubation steps the sample was read out *via* a laser scanner.

In this article we describe the further simplification and advancement of the MFA to a microfluidic compatible assay. We show for the first time the label-free detection of protein–DNA interactions *via* MFA. As a proof of principle, we used the binding of EcoRI, a restriction enzyme, to its DNA recognition site. Moreover we demonstrate the possibility for sensor size shrinking down to 5 µm × 5 µm. Now with the possibility of such a high density of different force probes, the label-free format and the wide range of detectable dissociation constants without restrictions the MFA shows the potential for DNA binding site screening with several advantages over the existing methods.

Molecular force assay

Below, the working principle and implementation of the MFA are described. Although the instrumentation is comparable to a microcontact printing setup, the key to the MFA lies within the molecular setup, the molecular force probes. The MFPs are assembled as follows: one strand, oligomer **1**, is connected to a glass support, the bottom surface, *via* a (hexaethyleneglycol)$_5$ spacer. The complementary strand, oligomer **2**, which also carries a Cy5 fluorescence label, possesses an overhang containing the sequence for the reference duplex **2·3**. The complementary DNA strand, oligomer **3**, carries a Cy3 dye on the one site and is biotin-modified at the end of a polythymine linker and completes the **1·2·3** complex on the glass slide. As a result two duplexes, **1·2** (target duplex) and **2·3** (reference duplex), are assembled and connected in series with a fluorescent label (Cy5) in between. Cy3 and Cy5 of strands **3** and **2** are in close proximity (7nt ssDNA) forming a FRET pair. The PDMS surface of the stamp is functionalized with streptavidin attached to 3400 g mol^{-1} PEG linkers.

Fig. 1a illustrates the very basic principle on a molecular level as the assay successively processes. At the beginning of the experiment the MFPs are attached to the glass slide but are still separated from the soft PDMS stamp. First the Cy5 is excited and the fluorescence signal of the MFP layer is measured ($F_A{}^A$). Secondly the Cy3 is excited and the fluorescence signal of Cy5 is measured ($F_D{}^A$). After readout the PDMS surface is brought in contact with the glass slide, allowing for biotin·streptavidin complexation; thus, the MFPs are grafted in parallel between both surfaces. After 10 min, the surfaces are separated at a constant velocity. Thereby the polymeric anchors are stretched and a force builds up gradually until the chain of molecular complexes ruptures either at the **1·2** or **2·3** duplex. So the unbinding force of each target DNA duplex is compared individually against a separate reference duplex. The biotin·streptavidin complex persists, since under our experimental conditions a 30 bp DNA duplex unbinds at around 40 to 50 pN, whereas biotin·streptavidin unbinds under these conditions beyond 100 pN.[16,27–29] The typical number of bp per DNA duplex used in our studies is limited by the thermal dissociation rate to around 15 bp at room temperature in 1× PBS. The stamp is moved away from the surface and the fluorescence signals $F_A{}^A$ and $F_D{}^A$ on the glass slide are read out a second time. Depending if the bond between **2·3** or **1·2** ruptures, strand **2** with its Cy5 fluorophore ends up on the glass slide or PDMS stamp. The result, *i.e.*, the fractions of broken target and broken reference bonds, is stored in a binary fluorophore distribution; fluorophore on the top or bottom surface. So the number of remaining Cy5 fluorophores reflects the relative difference in mechanical stability of the target duplexes compared to the reference duplexes. The number of Cy5 fluorophores is proportional to the measured intensity.[24] Finally, to correct for MFPs, which did not couple to the PDMS surface (Fig. 1a, third MFP from the right), DNA oligomer **3** is modified with a Cy3 label at the end close to Cy5 to form a FRET pair. After separation this FRET pair on the bottom surface is only intact, when the MFP was not probed and strand **3** is still attached to the MFP. To readout the signal of the FRET pair Cy3 is excited and the emission of the acceptor Cy5 is detected. Because forced bond rupture is a thermally assisted process and the force detector is limited by thermal noise, several hundred experiments are typically performed in single molecule force spectroscopy to determine the rupture forces with sufficient accuracy.[23,30] Here, we probe approximately 10^4 duplicates of these MFPs per µm^2 in parallel in a single experiment.

Technical implementation

In Fig. 1b the technical implementation is illustrated. The DNA chip consists of a 4 × 4 pattern of spots (diameter 1–2 mm) with
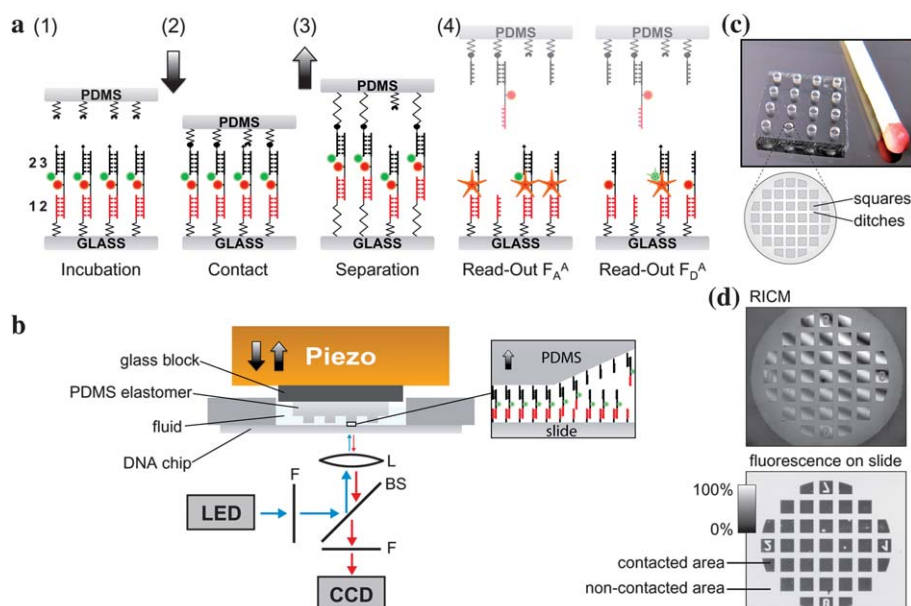
Fig. 1 Molecular force assay based on soft-print lithography. (a) Schematic representation of the MFA on a molecular level showing the basic principle and successively the assay processes. (a1) The molecular force probes (MFPs) are anchored *via* DNA strand **1** to the glass support. Each MFP comprises of 3 DNA strands. These 3 DNA strands hybridize in two DNA duplexes, **1·2** and **2·3**, coupled in series. DNA strand **2** carries a Cy5 as fluorescent marker and strand **3** a Cy3. The PDMS surface and the glass surface are still separated. (a2) The PDMS stamp is moved down to contact the glass surface. Thereby the biotin on DNA strand **3** couples to the streptavidin of the PDMS stamp and thus forms a bridge between the glass and PDMS. (a3) The surfaces are separated and a force builds up along both DNA duplexes of the MFPs until one of the two DNA duplexes ruptures. (a4) To count the number of intact, remaining **1·2** duplexes, the glass slide is readout *via* the fluorescence Cy5 dye on strand **2**. During the readout the PDMS stamp is far out of the focal plane. In the last step Cy5 is excited *via* FRET to mark all MFPs that did not couple to the PDMS stamp while in contact. (b) The fluid well with the DNA chip was placed in the contact device with PDMS stamp and detection system. A piezoelectric actuator moves the PDMS stamp along the *z*-axis to contact the DNA-chip. A standard fluorescence microscope with LED illumination and CCD camera is used to read out the sample. (c) The PDMS stamp consists of 16 pads. Each pad has a diameter and height of 1 mm. The microstructure on a pad comprises 100×100 μm squares with an elevation of 5 μm. The trenches between the squares are about 41 μm wide. (d) The planar adjustment between stamp and DNA chip as well as the contact process is controlled *via* reflection interference contrast microscopy. After contact, the fluorescence readout gives quantitative information about the ratio of broken reference and target duplexes.

different MFPs matching the pads of the soft PDMS stamp (Fig. 1c). The glass slide is attached to a PMMA well with silicone lip seal and fixed on a stainless steel stage with permanent magnets. The PDMS elastomer is placed upside down on a glass block connected vertically to a closed-loop piezoelectric actuator (PZ 400, Piezo Systems Jena, Germany) and a DC motorized translation stage (Physik Instrumente GmbH, Germany). The whole contact device is mounted on an inverted microscope (Axio Observer Z1, Carl Zeiss MicroImaging GmbH, Germany) with an *xy* DC motorized high-accuracy translation stage (Physik Instrumente GmbH, Germany). The planar adjustment between stamp and DNA chip as well as the contact process (Fig. 1d) are controlled *via* reflection interference contrast microscopy.[31]

One novel advancement is the direct readout of the DNA chip placed in the contact device. First it allows the fluorescence readout of the sample directly before and after the contact process in buffer solution without any stringent washing steps as done previously. Due to the diminishment of the systematic error caused by washing steps, the reproducibility and robustness of the experiment could be improved further. Secondly we could move away from the confocal microarray scanner to epi-fluorescence microscopy, which has several advantages including a simpler setup, improved signal-to-noise ratio and an elevated

reliability against surface inhomogeneities as depicted later. High-power LEDs (Philips Lumileds Lighting Comp. CA) were used for illumination. A simple cooling system composed of heat sink and fans combined with low-noise current drivers stabilizes the intensity of the LEDs with less than per mil deviation per hour. A standard CCD camera (MRm, Carl Zeiss MicroImaging GmbH, Germany) was used for detection. The entire contact and detection process is semi-automated *via* customized control software (LabVIEW, National Instruments Germany GmbH).

Analysis

To determine the ratio between broken target and reference bonds, a more subtle analysis is required, since it cannot be assumed that all MFPs physically connect perfectly to both surfaces *via* the biotin·streptavidin bond. Uncoupled MFPs result in a background signal. In order to calculate the normalized fluorescence (NF) intensity the background signal caused by uncoupled MFPs has to be identified and subtracted from the latter one. For simplicity, the unlikely case that the biotin·streptavidin bond ruptures is not further considered, since the MFP remains in the state S0 (**1·2·3**) and does not affect the final result. The NF is defined as the ratio between broken reference bonds and the total amount of MFPs that have been

under load. The detailed derivation for the NF has been given previously.[24] In short: initially, all molecular setups are present in the state S0 and were detected *via* the Cy5 labeled oligomer **2** (Fig. 1(a1)). After separation, the molecular setups on the glass slide exist in three different states, S0 (**1·2·3**), S1 (**1·2**), and S2 (**1**), as shown in Fig. 1(a4). An unbinding force was applied only to the molecular setups in states S1 and S2. Molecular setups in state S0 did not couple to the PDMS streptavidin surface and therefore retained the Cy3 labeled oligomer **3**. Because S1 and S0 cannot be distinguished only by Cy5, the MFPs in state S0 are identified *via* the signal of the FRET pair Cy3/Cy5. The F_A^A and F_D^A fluorescence images allow the quantification of the relative amounts of S0, S1, and S2.

$$NF = \frac{S1}{S1 + S2} = \frac{(F_A^A)_{ratio} - (F_D^A)_{ratio}}{1 - (F_D^A)_{ratio}}$$

Therefore the F_A^A final image (after contact) is divided by the F_A^A start image (Fig. 2). Thus not only the Gaussian illumination profile but also inhomogeneities in the MFP layer cancel out perfectly. Afterwards the resulting $(F_A^A)_{ratio}$ image is corrected for bleaching by normalizing the non-contacted areas to 1. In the same way the F_D^A final image is divided by the F_D^A start image and normalized to obtain the $(F_D^A)_{ratio}$ image that reflects the coupling efficiency.

Miniaturization

Typical force-histograms in single molecule force spectroscopy comprise normally of a few hundreds to thousands of force measurements to achieve an adequate force distribution to determine a mean value of force. On the other hand as mentioned in the last paragraph the density of MFPs is around 10^4 per μm^2. So the question arises: what is the minimum spot-size of the MFPs at a given signal to noise ratio? Fig. 3a shows a normalized fluorescence image (2 s exposure time, 63× objective). One can easily recognize the area that was contacted by the microstructure of the PDMS-stamp. The histogram in Fig. 3b depicts the NF of an entire 100 μm × 100 μm area in red and a 5 μm × 5 μm area in blue (blue square in Fig. 3a). For a more detailed conclusion the 5 μm × 5 μm ROI was moved in 5 μm steps over the 100 μm × 100 μm area. The mean NF values of each Gaussian fit of each 5 μm × 5 μm ROI are shown in the inset

histogram of Fig. 3b. The vertical dashed lines at NF = 0.405 and NF = 0.438 are the percentiles of 5% and 95%. For a further investigation a MFP-microarray with a spot-size of approximately 30 μm was contacted with the PDMS-surface in a way that a different large fraction of each spot was probed as shown in Fig. 3c and d. The probed areas "A" to "D" have different sizes since they were contacted by different areas of the PDMS-square (at the middle, the etches and at the corner). Though, the mean values of NF of the histograms "A" to "D" match very precisely. As a result we conclude that even a feature size as small as a few micrometres is sufficient to achieve the meaningful NF and standard deviation.

Detection of protein–DNA interactions

Force-based ligand detection in general relies on the shift of the unbinding forces due to receptor·ligand complex formation. In the same way the force-based ligand detection *via* MFA is based on a shift of mechanical stability due to DNA·ligand complex formation of one of the two DNA-duplexes (target duplex). Thereby the second duplex may be designed such that it does not bind ligand and therefore serves as a reference duplex. The molecular design can be seen as a well adjusted force balance which is detuned by the interaction of one of the balance arms with a ligand. Fig. 4a and b depict the basic principle in detail: without loss of generality in a perfect constructed MFP both DNA-duplexes comprise the same mechanical stability for a given force loading rate and the NF = 0,5. The target duplex—here, the lower DNA-duplex—carries a recognition site for a specific ligand and the reference duplex (upper bond) does not. Upon binding of the ligand to its recognition site, only the mechanical stability of the target duplex is altered. This leads to an imbalance and a shift in NF. Since the MFA is capable of detecting changes in the range of a few pN,[21] even the smallest changes in stability due to complexation result in a detectable shift in NF. As depicted in Fig. 4c and d it is possible to construct the MFPs in a shear (Fig. 4c) and a zipper-like pulling geometry (Fig. 4d). As shown with AFM the shear geometry comprises a reference force of around 60 pN for a 30 bp DNA duplex at moderate loading rates.[27,29] In comparison with that, in zipper
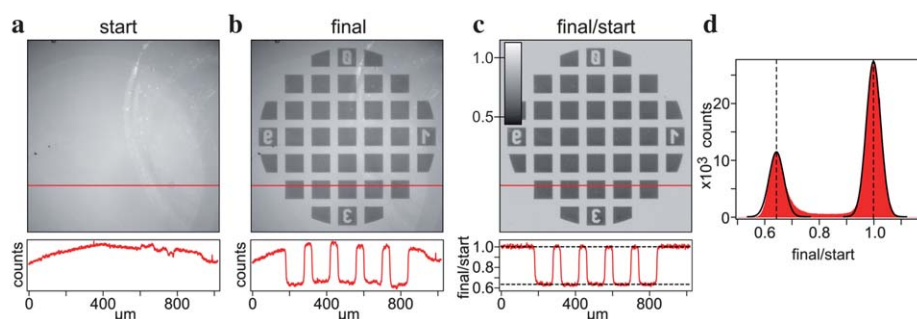

Fig. 2 Pixel-by-pixel analysis accomplished through image division. The fluorescence images (Cy5, exposure time 2 s) show a distinct ROI on the DNA-chip before (a) and after contact (b). (c) After background subtraction from images (a) and (b), image (b) is divided through image (a). As a result illumination curvature as well as artifacts and inhomogeneities in the MFP layer are perfectly corrected. In the last step, this image is corrected for fluorophore bleaching, so that the non-contacted area is normalized to 1. The intensities measured in the contacted areas give the fraction of remaining fluorophores respectively the intact lower DNA duplexes of the MFPs on the DNA-chip. (d) Histogram of image (c). Here, 64% of the lower DNA duplexes of the MFPs are still intact on the DNA-chip.
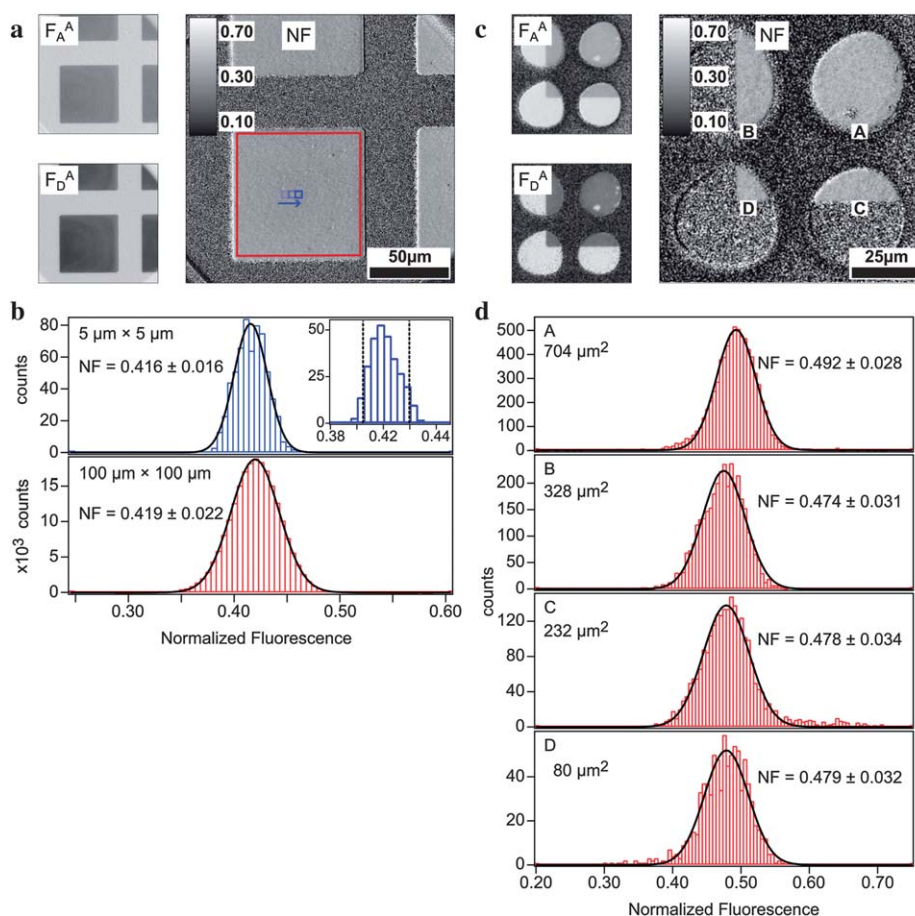
Fig. 3 Miniaturization of the MFA. (a) Fluorescence images F_A^A and F_D^A (63× objective, 2 s exposure time). On the right the calculated NF image; a blue square marks a ROI of 5 μm × 5 μm. (b) Histogram of (a): in red a 100 μm × 100 μm square of the microstructure (NF = 0.419 ± 0.022), in blue the 5 μm × 5 μm ROI (NF = 0.416 ± 0.016). The inset histogram shows the distribution of mean NF values as the 5 μm × 5 μm ROI was moved in 5 μm steps over the entire 100 μm × 100 μm area. The vertical dashed lines at NF = 0.405 and NF = 0.438 are the percentiles of 5% and 95%. (c) Fluorescence images F_A^A and F_D^A (40× objective, 1 s exposure time) of a MFP-microarray. On the right the calculated NF image. All spots of the microarray are composed of the same kind of MFPs to compare the influence of the geometry of the PDMS surface with the NF. The PDMS-square has contacted in such a way 4 spots of the MFP-microarray that the spots feature varied sizes of contacted areas. (d) Histogram of (c): for all 4 spots the whole contacted area is plotted in histograms. Even spot "D" (80 μm²), which was contacted with the corner of the PDMS-square, matches very precisely the mean NF of the other 3 spots. The possibility to scale the MFA to a few micrometres down opens the opportunity to incorporate the MFA as sensor in microfluidics. Furthermore it is now possible to build MFA arrays with a very high density comparable to microarray technology.

geometry, the DNA duplex ruptures depending on the base content and composition at around 15 pN in a quasi-equilibrium process.[32,33] Hence the zipper geometry allows the design of an even more sensitive force sensor compared to shear geometry.

As a model system we chose the binding of EcoRI, a type II restriction endonuclease, to its DNA recognition sequence. In *Escherichia coli*, EcoRI serves as a protection system against foreign DNA and cleaves in the presence of Mg^{2+} ion cofactor, its unmethylated target sequence. Restriction endonucleases exhibit high affinities with dissociation constants in the low nM range concomitant with a very high sequence specificity. Under physiological salt conditions, the ratio of specific to non-specific binding of EcoRI reaches 10^9.[34–37] EcoRI binds in the absence of Mg^{2+} ion cofactor as a dimer to the palindromic DNA target site 5′-GAATTC-3′. Commercial grade EcoRI (32 kDa per monomer, 2×10^6 U mg^{-1} specific activity, 100 000 U ml^{-1} stock concentration) was purchased from NEB and used directly

without further purification. If not indicated otherwise, all experiments were performed at room temperature in the same buffer solution composed of 10 mM Hepes, 50 μM DTT, 100 μg ml^{-1} BSA, 170 mM NaCl and 1 mM EDTA at a pH of 7.6. The typical sample volume was 40 μl per PDMS-pad for a high degree of reproducibility. The minimum sample volume needed is 5 μl per PDMS-pad. First the EcoRI monomer concentration of the stock solution was determined twice *via* a quantitative SDS-PAGE to 100 nM with good reproducibility. Secondly we checked the affinity of EcoRI to the DNA constructs **1·2** and **2·3** *via* electrophoretic mobility shift assay (EMSA). Only the target duplex **1·2** exhibits strong binding to EcoRI with a $K_D = 1.8 \pm 1.0$ nM, whereas the reference duplex **2·3** did not show any binding in the whole accessible range from 0 nM to 50 nM EcoRI. The MFA measurements were carried out as follows: prior to measurement the DNA-chip was incubated with EcoRI for at least 2 hours. In Fig. 5 two MFA titration curves for
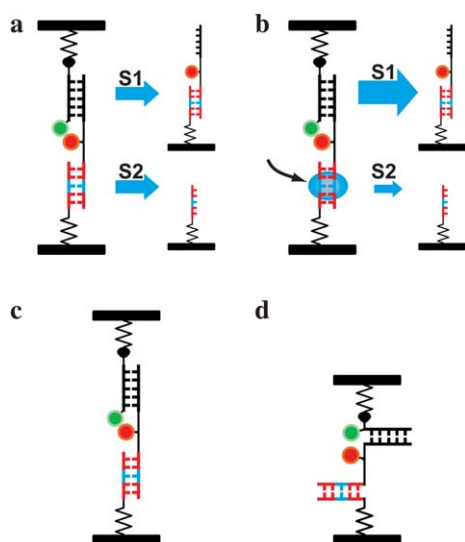
Fig. 4 The principle of ligand detection *via* MFA. The lower DNA-duplex comprises a target sequence for ligand binding, the upper one is the reference duplex without binding site. (a) In a perfect constructed MFP the lower and upper DNA-duplex have the same mechanical stability and the rupture probabilities for the duplexes S1 and S2 are the same. (b) If a ligand is bound to the lower DNA-duplex, the mechanical stability of that duplex is altered and the probability, that the reference duplex ruptures, shifts (typically: S1 > S2). Furthermore the MFP can be assembled in different geometries allowing unbinding forces to shear the DNA duplex in the range of 50 to 60 pN (c) or to unzip the duplex at around 15 pN (d).

different pulling geometries are presented. The graph in Fig. 5a depicts the change in NF against the EcoRI concentration. The target site for EcoRI is in the lower DNA-duplex. The upper reference duplex does not contain any binding site for the enzyme. The pulling direction of the MFP is in shear geometry on the 5′-ends of the DNA. The pulling velocity was 5 μm s⁻¹. The data were fitted by a hill equation isotherm, since EcoRI binds as a homodimer to its DNA recognition site: NF_{min} = 0.46 ± 0.01, NF_{max} = 0.88 ± 0.01 and K_D = 0.97 ± 0.14 nM. In zipper configuration (Fig. 5b) with different pulling velocities of 100 nm s⁻¹ (cycles) and 5 μm s⁻¹ (filled cycles) the fit of the data resulted in NF_{min} = 0.74 ± 0.01, NF_{max} = 0.95 ± 0.01 and K_D =

0.22 ± 0.06 nM. So the NF in both cases rose with increasing EcoRI concentration until saturation. Longer incubation times (up to 24 hours) did not further increase the NF. The K_D values from the MFA are in very good agreement with literature.[12] The K_D value obtained from EMSA is slightly higher than both MFA measurements, which might be due to different conditions caused by the gel in the EMSA.

Optical tweezer experiments have shown that the stability of the EcoRI: DNA bond is not influenced by the unzipping of the neighboring DNA bases even at slow loading rates down to 10 pN s⁻¹.[12,38] In shear geometry, however, all bases in the DNA duplex are loaded simultaneously and the structure of the DNA duplex might change prior to rupture, *e.g.* by unwinding, which might detach the bound protein with a certain probability from the DNA before the duplex itself ruptures.

As already described previously,[24] it is essential to compare the timescale of the thermal dissociation of the complex with the timescale of the force loading rate. If the system is allowed to equilibrate during the force ramp, the external force shifts the equilibrium away from the complex, which would result in an increased apparent KD. The lifetime or inverse dissociation rate for an EcoRI·dsDNA complex was experimentally determined to be in the order of tens of seconds.[39] At 5 μm s⁻¹ separation velocity and similar linker lengths, the force needed to rupture a 30 bp DNA duplex is built up on timescales in the order of t = 10 ms.[27] The DNA duplex unbinding occurs therefore on a much faster timescale t than the association or dissociation of the EcoRI·dsDNA complex at relevant ligand concentrations. Furthermore as shown for the zipper configuration the NF did not depend on pulling velocity corroborating our assumption that the rupture process of DNA unzipping occurs close to equilibrium.[33,40] This independency of the pulling velocity in the zipper configuration enhances the reproducibility of the MFA for quantitative ligand detection, since the detachment velocity of the stamp must not be controlled exactly.

Discussion and outlook

In the present article we have demonstrated a molecular force assay for the detection of protein–DNA interactions. The assay is based on the direct comparison of unbinding forces of
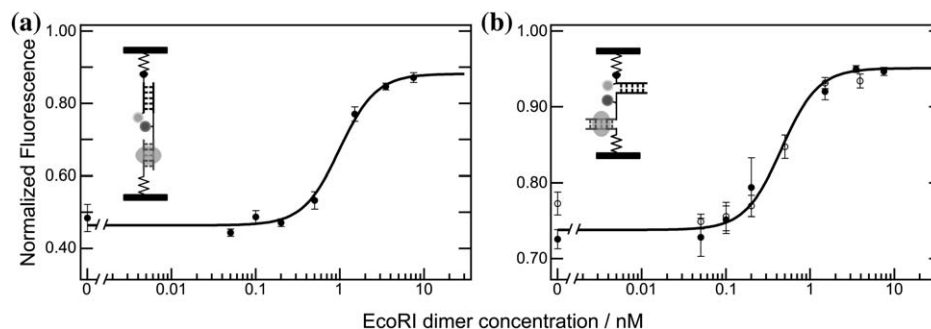

Fig. 5 Detection of protein–DNA interactions at physiological conditions. The restriction enzyme EcoRI binds as homodimer to its DNA target sequence 5′-GAATTC-3′. The target site for EcoRI is in the lower DNA-duplex. The upper DNA duplex does not contain any binding site for the enzyme and serves as reference duplex. (a) Pulling direction of the MFP in shear geometry at the 5′-ends of the DNA. The pulling velocity is 5 μm s⁻¹. The NF rises with increasing EcoRI concentration until saturation. The data are fitted by a hill equation isotherm: NF_{min} = 0.46 ± 0.01, NF_{max} = 0.88 ± 0.01, K_D = 0.97 ± 0.14 nM. (b) MFPs in zipper geometry with different pulling velocities of 100 nm s⁻¹ (cycles) and 5 μm s⁻¹ (filled cycles). NF_{min} = 0.74 ± 0.01, NF_{max} = 0.95 ± 0.01, K_D = 0.22 ± 0.06 nM.

biomolecules at the single molecule level in a highly parallel format, which allows the direct readout of roughly 10^4 molecular force probes per μm^2. Besides the highly parallel format and the scalability, the major advantage of the MFA lies in the detection of interaction forces between specific molecules. Not the presence of a certain binder, but rather its interaction strength is measured, which allows the discrimination between the specific interaction of interest and non-specific binding to the surface.

In this article we introduced a new low cost and easy to use setup, which allows force measurement and optical readout on the same instrument with a very high degree of reproducibility and enhancement in simplification of the measurement process. For this purpose we implemented a FRET pair in the molecular force probes to determine the ratio of MFPs under load. For the optical readout, standard epi-fluorescence was employed with LED illumination and a simple CCD camera for detection. The combination of both features leads to a robust biomolecular sensor based on unbinding forces. Besides the technical development we presented for the first time the detection of protein–DNA interactions and the quantification of the corresponding dissociation constant *via* the MFA. In addition we demonstrated successfully ligand detection with different pulling geometries of molecular force probes and advantages of the DNA zipper geometry for ligand detection. Moreover, we could show that a feature size as small as 5 $\mu m \times$ 5 μm is sufficient to determine the NF. For this, it follows that the MFA is capable of screening for protein–DNA interactions comparable to PBMs, ChIP-chip and MITOMI. Compared to these high-throughput methods the following advantages arise: (i) no stringent washing between force measurement and readout is needed, (ii) a wide range of affinities is accessible, even weak binders,[26] (iii) a quantitative and robust analysis due to the simple image division for normalization, (iv) and no label or marker against the protein is needed since the MFA relies on the detection of the specific interaction of binding protein and DNA.

In summary, the MFA has the potential to evolve to a new and valuable tool for the screening of biomolecular interactions with several advantages due to its force-based detection principle. In the future the MFA will be extended to different kinds of biomolecular interactions like protein–protein interactions and will be implemented or combined with microfluidic devices.

Acknowledgements

References

1 V. Iyer, C. Horak, C. Scafe, D. Botstein, M. Snyder and P. Brown, *Nature*, 2001, **409**, 533–538.
2 B. Ren, F. Robert, J. Wyrick, O. Aparicio, E. Jennings, I. Simon, J. Zeitlinger, J. Schreiber, N. Hannett, E. Kanin, T. Volkert, C. Wilson, S. Bell and R. Young, *Science*, 2000, **290**, 2306–2309.
3 A. R. Wu, J. B. Hiatt, R. Lu, J. L. Attema, N. A. Lobo, I. L. Weissman, M. F. Clarke and S. R. Quake, *Lab Chip*, 2009, **9**, 1365–1370.
4 M. F. Berger, A. A. Philippakis, A. M. Qureshi, F. S. He, P. W. Estep and M. L. Bulyk, *Nat. Biotechnol.*, 2006, **24**, 1429–1435.
5 S. Mukherjee, M. F. Berger, G. Jona, X. S. Wang, D. Muzzey, M. Snyder, R. A. Young and M. L. Bulyk, *Nat. Genet.*, 2004, **36**, 1331–1339.
6 M. L. Bulyk, *Curr. Opin. Biotechnol.*, 2006, **17**, 422–430.
7 T. Lee, N. Rinaldi, F. Robert, D. Odom, Z. Bar-Joseph, G. Gerber, N. Hannett, C. Harbison, C. Thompson, I. Simon, J. Zeitlinger, E. Jennings, H. Murray, D. Gordon, B. Ren, J. Wyrick, J. Tagne, T. Volkert, E. Fraenkel, D. Gifford and R. Young, *Science*, 2002, **298**, 799–804.
8 C. Harbison, D. Gordon, T. Lee, N. Rinaldi, K. Macisaac, T. Danford, N. Hannett, J. Tagne, D. Reynolds, J. Yoo, E. Jennings, J. Zeitlinger, D. Pokholok, M. Kellis, P. Rolfe, K. Takusagawa, E. Lander, D. Gifford, E. Fraenkel and R. Young, *Nature*, 2004, **431**, 99–104.
9 E. Segal, T. Raveh-Sadka, M. Schroeder, U. Unnerstall and U. Gaul, *Nature*, 2008, **451**, 535–540.
10 S. J. Maerkl and S. R. Quake, *Science*, 2007, **315**, 233–237.
11 F. Bartels, B. Baumgarth, D. Anselmetti, R. Ros and A. Becker, *J. Struct. Biol.*, 2003, **143**, 145–152.
12 S. J. Koch, A. Shundrovsky, B. C. Jantzen and M. D. Wang, *Biophys. J.*, 2002, **83**, 1098–1105.
13 F. Kuhner, L. Costa, P. Bisch, S. Thalhammer, W. Heckl and H. Gaub, *Biophys. J.*, 2004, **87**, 2683–2690.
14 A. R. Bizzarri and S. Cannistraro, *Chem. Soc. Rev.*, 2010, **39**, 734–749.
15 Y. Cao, M. M. Balamurali, D. Sharma and H. Li, *Proc. Natl. Acad. Sci. U. S. A.*, 2007, **104**, 15677–15681.
16 R. Merkel, P. Nassoy, A. Leung, K. Ritchie and E. Evans, *Nature*, 1999, **397**, 50–53.
17 V. Moy, E. Florin and H. Gaub, *Science*, 1994, **266**, 257–259.
18 K. Uhrig, R. Kurre, C. Schmitz, J. E. Curtis, T. Haraszti, A. E.-M. Clemen and J. P. Spatz, *Lab Chip*, 2009, **9**, 661–668.
19 C. H. Albrecht, K. Blank, M. Lalic-Mülthaler, S. Hirler, T. Mai, I. Gilbert, S. Schiffmann, T. Bayer, H. Clausen-Schaumann and H. E. Gaub, *Science*, 2003, **301**, 367–370.
20 K. Blank, T. Mai, I. Gilbert, S. Schiffmann, J. Rankl, R. Zivin, C. Tackney, T. Nicolaus, K. Spinnler, F. Oesterhelt, M. Benoit, H. Clausen-Schaumann and H. Gaub, *Proc. Natl. Acad. Sci. U. S. A.*, 2003, **100**, 11356–11360.
21 C. H. Albrecht, H. Clausen-Schaumann and H. E. Gaub, *J. Phys.: Condens. Matter*, 2006, **18**, 581–599.
22 F. Gittes and C. Schmidt, *Eur. Biophys. J.*, 1998, **27**, 75–81.
23 M. Viani, T. Schaffer, A. Chand, M. Rief, H. Gaub and P. Hansma, *J. Appl. Phys.*, 1999, **86**, 2258–2262.
24 D. Ho, C. Dose, C. H. Albrecht, P. Severin, K. Falter, P. B. Dervan and H. E. Gaub, *Biophys. J.*, 2009, **96**, 4661–4671.
25 C. Dose, D. Ho, H. E. Gaub, P. B. Dervan and C. H. Albrecht, *Angew. Chem., Int. Ed.*, 2007, **46**, 8384–8387.
26 D. Ho, K. Falter, P. Severin and H. E. Gaub, *Anal. Chem.*, 2009, **81**, 3159–3164.
27 J. Morfill, F. Kuehner, K. Blank, R. A. Lugmaier, J. Sedlmair and H. E. Gaub, *Biophys. J.*, 2007, **93**, 2400–2409.
28 F. Pincet and J. Husson, *Biophys. J.*, 2005, **89**, 4374–4381.
29 T. Strunz, K. Oroszlan, R. Schäfer and H. J. Güntherodt, *Proc. Natl. Acad. Sci. U. S. A.*, 1999, **96**, 11277–11282.
30 E. Evans and K. Ritchie, *Biophys. J.*, 1997, **72**, 1541–1555.
31 G. Wiegand, K. Neumaier and E. Sackmann, *Appl. Opt.*, 1998, **37**, 6892–6905.
32 C. Bustamante, Z. Bryant and S. Smith, *Nature*, 2003, **421**, 423–427.
33 M. Rief, H. Clausen-Schaumann and H. Gaub, *Nat. Struct. Biol.*, 1999, **6**, 346–349.
34 A. Jeltsch, J. Alves, H. Wolfes, G. Maass and A. Pingoud, *Biochemistry*, 1994, **33**, 10215–10219.
35 L. Jen-Jacobson, *Biopolymers*, 1997, **44**, 153–180.
36 D. R. Lesser, M. R. Kurpiewski and L. Jen-Jacobson, *Science*, 1990, **250**, 776–786.
37 N. Sidorova and D. Rau, *J. Mol. Biol.*, 2001, **310**, 801–816.
38 S. Koch and M. Wang, *Phys. Rev. Lett.*, 2003, **91**, 028103.
39 N. Sidorova and D. Rau, *Biopolymers*, 2000, **53**, 363–368.
40 C. Bustamante, S. Smith, J. Liphardt and D. Smith, *Curr. Opin. Struct. Biol.*, 2000, **10**, 279–285.